Unconventional quantum correlations of light emitted by a single atom in free space

D. Goncalves [1,*] M. W. Mitchell [1,2] and D. E. Chang [1,2]

[1]*ICFO-Institut de Ciencies Fotoniques, The Barcelona Institute of Science and Technology, 08860 Castelldefels (Barcelona), Spain*

[2]*ICREA-Institució Catalana de Recerca i Estudis Avançats, 08015 Barcelona, Spain*

(Received 28 April 2020; revised 2 October 2020; accepted 12 July 2021; published 29 July 2021)

We present an approach to engineer the photon correlations emerging from the interference between an input field and the field scattered by a single atom in free space. Nominally, the inefficient atom-light coupling causes the quantum correlations to be dominated by the input field alone. To overcome this issue, we propose the use of separate pump and probe beams, where the former increases the atomic emission to be comparable to the probe. Examining the second-order correlation function $g^{(2)}(\tau)$ of the total field in the probe direction, we find that the addition of the pump formally plays the same role as increasing the coupling efficiency, even though the physical atom-light coupling efficiency remains unchanged. We show that one can tune the correlation function $g^{(2)}(0)$ from zero (perfect antibunching) to infinite (extreme bunching) by a proper choice of pump amplitude. We further elucidate the origin of these correlations in terms of the transient atomic state following the detection of a photon, and show that these correlations can be observed under realistic conditions.

DOI: 10.1103/PhysRevA.104.013724

I. INTRODUCTION

Despite its apparent simplicity, the interference between an optical field incident on a single atom and the field scattered by such a quantum nonlinear element gives rise to a wealth of phenomena. For example, it can produce strong bunching or antibunching of the reradiated fields [1–3], or yield a "quantum aperture" for light with a rich spatial structure of quantum photon correlations [3]. It can also give rise to nontrivial stimulated emission statistics at the quantum level [4], induce multiphoton bound states in scattering [5,6], or produce photon-number-dependent propagation delays [7]. To realize the majority of these effects, however, it is necessary to achieve highly efficient interactions between individual photons and the atom, such that the incident light and rescattered fields become comparable in strength, leading to a large interference.

Unfortunately, the single photon-atom interaction efficiency is intrinsically weak in free space. For a single incident photon focused to an area A and with a wavelength λ resonant with the transition of a two-level atom, the interaction efficiency scales $\sim\lambda^2/A$ [3]. However, the diffraction limit ($A \gtrsim \lambda^2$) and subtleties associated with tight focusing [8,9] constrain this interaction probability to be about $\sim$10% in current experiments [10–12]. For such low coupling efficiencies, the total field is instead dominated by the (classical) input field. Thus far, the only routes towards unity coupling efficiency have involved either high-finesse cavities [13,14] or waveguides with strong-field confinement [15,16].

In this work, we present an approach to observe and manipulate quantum interference effects between an incoming field and a single free-space atom, even in the low coupling regime. The key idea is to use two separate pump and probe fields propagating in spatial modes that only significantly overlap at the atomic position (Fig. 1) [17]. Then, the total transmitted light collected in the probe direction consists of the input field and the quantum rescattered field, which contains contributions from both pump and probe beams. By tuning the pump strength, the total scattered field can become comparable to the probe amplitude, allowing for rich correlations to emerge. In particular, we show that, as far as the transmitted intensity and the second-order field correlation function $g^{(2)}(\tau)$, the addition of the pump formally plays the same role as increasing the coupling efficiency, even though the physical efficiency of probe photons interacting with the atom remains the same. This can be used to tune between fully antibunched [$g^{(2)}(0) \to 0$] and extremely bunched [$g^{(2)}(0) \to \infty$] second-order correlation functions of the total field. We also provide an interpretation of the physical origin of these correlations from the atomic state perspective. Finally, we also present some considerations to observe these effects under realistic experimental conditions.

II. THEORETICAL MODEL

Generally, our goal will be to calculate the spatiotemporal properties and correlations of a quantum field, as it propagates and interacts with an atom as in Fig. 1, for which we briefly present our theoretical formalism here. First, we consider the dynamics of an ideal, two-level atom with ground state $|g\rangle$ and excited state $|e\rangle$ driven by a resonant input field with Rabi frequency Ω representing the combination of classical probe and pump input beams. The time evolution of the quantum atomic state $\hat{\rho}$ obeys the master equation

$$\dot{\hat{\rho}} = -\frac{i}{\hbar}[\hat{H}, \hat{\rho}] + \frac{\Gamma_0}{2}(2\hat{\sigma}^{ge}\hat{\rho}\hat{\sigma}^{eg} - \hat{\sigma}^{ee}\hat{\rho} - \hat{\rho}\hat{\sigma}^{ee}), \quad (1)$$

*daniel.goncalves@icfo.es

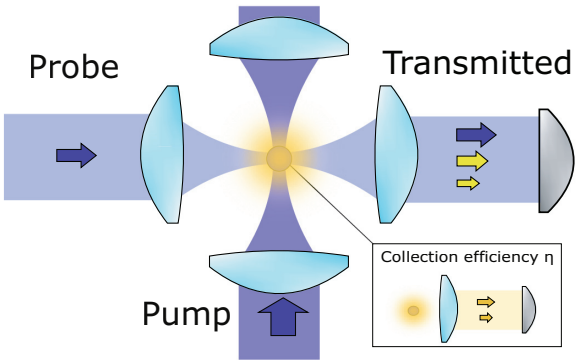

FIG. 1. Conceptual scheme of the proposed technique. Two coherent, continuous beams (pump and probe) illuminate resonantly a single atom in a "Maltese cross" configuration. Along the transmitted direction of the probe beam, the total field consists of the coherent sum of the incident probe field (small blue arrow) and the quantum field rescattered by the atom, which contains contributions from both the probe and pump beams (small and large yellow arrows, respectively). A sufficiently large pump beam allows the rescattered field to be comparable to the incident probe in intensity, despite a low collection efficiency η of emitted photons in the transmitted direction. This enables strong quantum correlations to emerge in the collected field.

where Γ_0 is the free-space spontaneous emission rate and $\hat{\sigma}^{ab} = |a\rangle\langle b|$ are atomic operators with $\{a, b\} \in \{e, g\}$. The Hamiltonian $\hat{H}$ from Eq. (1) contains the interaction term between the atom and a resonant, quantum driving field. Explicitly, it takes the form $\hat{H} = -\hbar(\Omega\hat{\sigma}^{eg} + \text{H.c.})$ in the laser's rotating frame. Whereas the spontaneous emission term of Eq. (1) implicitly encodes the loss of atomic excitation in the form of radiated photons, the explicit spatiotemporal properties of this rescattered field can be found through the input-output relation [18,19]

$$\hat{\mathbf{E}}_{\text{out}}(\mathbf{r}) = \hat{\mathbf{E}}_{\text{in}}(\mathbf{r}) + \mu_0\omega_{ge}^2\mathbf{G}_0(\mathbf{r}, \mathbf{r}_a, \omega_{ge}) \cdot \mathbf{d}_{ge}\,\hat{\sigma}^{ge}, \quad (2)$$

where $\hat{\mathbf{E}}_{\text{in}}(\mathbf{r})$ is the input field operator and $\mathbf{r}_a$ the position of the atom. The quantity $\mathbf{d}_{ge}$ is the dipole matrix element associated to the transition $|g\rangle \leftrightarrow |e\rangle$ with frequency ω_{ge} and is connected to Γ_0 through the relation $\Gamma_0 = |\mathbf{d}_{ge}|^2\omega_{ge}^3/(3\pi\hbar\epsilon_0 c^3)$ [20]. $\mathbf{G}_0(\mathbf{r}, \mathbf{r}_a, \omega_{ge})$ is the Green's function in free space, which encodes the field emitted by a pointlike dipole source and satisfies the electromagnetic wave equation [21]

$$\left[(\nabla \times \nabla \times) - \frac{\omega_{ge}^2}{c^2}\mathbb{1}\right]\mathbf{G}_0(\mathbf{r}, \mathbf{r}', \omega_{ge}) = \delta(\mathbf{r} - \mathbf{r}')\mathbb{1}. \quad (3)$$

Its explicit form is given by

$$\mathbf{G}_0(\mathbf{r}, \mathbf{r}', \omega_{ge}) = \frac{e^{ik_0R}}{4\pi R}\left[\left(1 + \frac{i}{k_0R} - \frac{1}{k_0^2R^2}\right)\mathbb{1} - \left(1 + \frac{3i}{k_0R} - \frac{3}{k_0^2R^2}\right)\frac{\mathbf{R}\otimes\mathbf{R}}{R^2}\right], \quad (4)$$

where $R = |\mathbf{r} - \mathbf{r}'|$ and $k_0 = \omega_{ge}/c$. The tensor nature of the Green's function accounts for the vectorial nature of both the dipole source orientation and the emitted field. Equation (2) states that the total field can be decomposed into an incident field and a field rescattered by the atom, an idea well known in classical optics. Importantly, however, such a relation also holds true as an operator equation. In particular, it enables the quantum correlations of the output field $\hat{\mathbf{E}}_{\text{out}}(\mathbf{r})$ to be calculated in terms of the input field and atomic state [the latter being encoded in the solution to Eq. (1)].

Although Eq. (2) is formally true, measuring the fields at a single point $\mathbf{r}$ is not typical from an experimental perspective. One commonly used detection modality consists of collecting the transmitted light through the atom with an optical imaging system, which projects the total field into a certain spatial mode. To provide a specific example, in Fig. 1, the probe field might consist of a focused Gaussian beam, while in the transmitted direction, light is collected back into the same Gaussian mode. Assuming that the input and detection spatial mode $\mathbf{E}_{\text{det}}(\mathbf{r})$ are the same, one can project the operator $\hat{\mathbf{E}}_{\text{out}}(\mathbf{r})$ from Eq. (2) into this preferred mode to obtain (see the Appendix) [22]

$$\hat{E}_{\text{det}} = \hat{E}_{\text{in,det}} + i\sqrt{\eta\Gamma_0}\,\hat{\sigma}^{ge}, \quad (5)$$

where $\hat{E}_{\text{in,det}}$ is the input field in the detection mode. Here, we have rescaled the field operators such that $\langle\hat{E}_{\text{det}}^\dagger\hat{E}_{\text{det}}\rangle$ represents the total number of photons per unit time. According to Eq. (5), the total field $\hat{E}_{\text{det}}$ is the coherent sum of the input field and the field rescattered by the atom, which allows for interference phenomena to emerge. The second term in Eq. (5) only accounts for the fraction of atomic emission captured by the detector, as the atom continues to spontaneously emit light into all directions (not only the specific mode we measure), yielding the atomic relaxation in Eq. (1). As discussed in the Appendix, the validity of Eq. (5) requires that the local phase of the detection mode at the atomic location is gauged away into the definition of $\hat{\sigma}^{ge}$ itself. From a practical perspective, this is equivalent to enforcing that the Rabi frequency associated with the detection mode is always chosen to be real and positive. The projection of the scattered field into the detection mode is encoded in a single parameter, η, which physically describes the collection efficiency of a single emitted photon into this mode. By time-reversal symmetry, it also provides the interaction efficiency between the atom and an incoming resonant photon [23,24]. In both cases, η is a purely geometric quantity that only depends on the overlap between a specific mode and the dipole radiation pattern, and is thus independent from the strength of the fields.

The formal procedure to obtain η given some detection mode is described in the Appendix. As an example, let us consider a Gaussian beam of waist w_0 polarized in the direction of the dipole matrix element. The spatial dependence of said Gaussian mode is given by [20]

$$E(\rho, \zeta) = E_0\frac{w_0}{w(\zeta)}\,e^{-\rho^2/w(\zeta)^2}\,e^{-i[k_0\zeta + \Phi(\zeta,\rho)]} \quad (6)$$

in the paraxial approximation. Here, ρ is the radial distance from the center axis of the beam and ζ is the coordinate along the direction of propagation. By conveniently choosing the atomic position to coincide with the focal point, we find the well-known result $\eta \approx 3\lambda^2/8\pi^2 w_0^2$ (see the Appendix) [3]. One could go beyond the paraxial approximation to account for different corrections, such as the distortion of the

polarization due to tight focusing of the beams [9] or details related to the focusing lens [8]. However, for small values of η, i.e., low focusing, the paraxial approximation agrees very well with full vector solutions [25]. In any case, our results below will be given in terms of η to be as general as possible, and thus are independent of such considerations.

III. PUMP-PROBE SCHEME

Having introduced a rather general formalism to calculate the properties of the quantum field, we now apply it specifically to the pump-probe scenario introduced earlier. As a first step, we explore how the pump modifies the transmission of light in the probe mode.

A. Transmission in the collection direction

Following the discussion from Sec. II, our strategy will be to first obtain the atomic state driven by the total field [Eq. (1)] and use it to construct field correlations according to Eq. (5). Although the single-atom density matrix can be readily solved in general, here we focus on the weak driving regime where $|\Omega| \ll \Gamma_0$, which already contains the interesting physics. In this limit, to lowest order, the steady-state solution of Eq. (1) is $\hat{\rho}_{eg} \approx 2i\Omega/\Gamma_0$ for the atomic coherence and $\hat{\rho}_{ee} \approx |\hat{\rho}_{eg}|^2$ for the excited population. Their specific values depend on the Rabi frequency of the total field driving the atom, which is the admixture of the pump and the probe contributions, $\Omega = \Omega_{\text{pump}} + \Omega_{\text{probe}}$. As previously discussed, by convention and for Eq. (5) to be valid, we impose $\Omega_{\text{probe}} > 0$ to be real and positive, while allowing $\Omega_{\text{pump}} = |\Omega_{\text{pump}}|e^{i\phi}$ to be complex.

Once the atomic state is known, we calculate the transmission of light in the probe mode. We assume that the pump beam is in a completely orthogonal mode to the probe, such that its contribution to the detected field in Eq. (5) only comes via the atomic scattered field. We define the transmission coefficient T as the ratio between intensities seen in the detection mode and the probe input, i.e., $T = \langle \hat{E}^\dagger_{\text{det}} \hat{E}_{\text{det}} \rangle / \langle \hat{E}^\dagger_{\text{in,det}} \hat{E}_{\text{in,det}} \rangle$. It can be shown that, for normally ordered correlation functions and coherent state inputs, the input field operator $\hat{E}_{\text{in,det}}$ in Eq. (4) can be replaced by the square root of its corresponding coherent state photon flux $\sqrt{\Phi_{\text{p}}}$ [26], according to our normalization for the operators. Substituting Eq. (5) into the definition for the transmission coefficient, we find

$$T = 1 - 2\sqrt{\eta\Gamma_0}\frac{\text{Im}\{\hat{\rho}_{eg}\}}{\sqrt{\Phi_{\text{p}}}} + \eta\Gamma_0\frac{\hat{\rho}_{ee}}{\Phi_{\text{p}}}, \tag{7}$$

which explicitly depends on the atomic coherence and population in the excited state, for which we substitute the aforementioned values in the weak driving regime. The resulting expression contains both Ω_{probe} and the probe photon flux Φ_{p}, which are related through $\eta\Phi_{\text{p}} = |\Omega_{\text{probe}}|^2/\Gamma_0$ (see the Appendix). With this, it is straightforward to show that

$$T = |1 - 2\Lambda|^2, \tag{8}$$

where $\Lambda = \eta\Omega/|\Omega_{\text{probe}}|$ is an effectively enhanced coupling parameter that depends on three quantities: the ratio $|\Omega_{\text{pump}}|/|\Omega_{\text{probe}}|$, the pump-probe relative phase ϕ, and the free-space atom-photon coupling efficiency η.

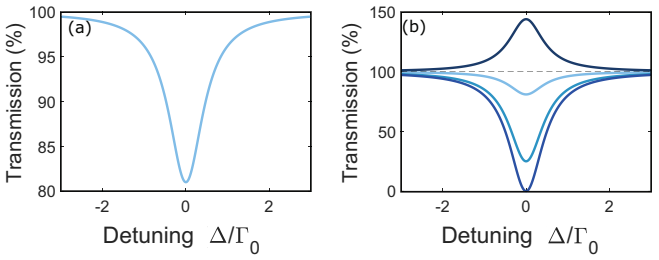

FIG. 2. Transmission spectra of a weak, coherent probe beam as a function of the laser detuning Δ from the atomic resonance, in units of the free-space decay rate Γ_0. (a) Transmission spectrum without the pump. We take a realistic coupling efficiency of $\eta = 0.05$, consistent with typical experimental values. (b) Same as (a) but now with the additional pump beam, with pump-probe relative phase $\phi = 0$. The pump amplitude is tuned to obtain different effective coupling efficiencies $\Lambda = \{\eta, 0.25, 0.5, 1.1\}$ (colors from light to dark blue). We note a total extinction of the resonant transmission for $\Lambda = 0.5$ and transmission higher than 100% for $\Lambda > 1$.

We now discuss the implications of Eq. (8) starting with the case without the pump beam, where the transmission takes the well-known value $T = |1 - 2\eta|^2$ for single-atom resonant transmission [2,12,27]. For small η, light is only weakly attenuated as the atom scatters a small fraction of the incoming photons into arbitrary directions. As a result, interference between incident and scattered fields in Eq. (5) is necessarily destructive and $T \leqslant 1$. In the hypothetical (but unrealistic [9]) case that the probe mode could be made to cover an entire half-space of solid angle, and moreover match the atomic dipole emission pattern, the coupling efficiency would reach its theoretical maximum value $\eta = 1/2$ for the setup in Fig. 1, yielding perfect attenuation $T = 0$. Interestingly, by introducing the pump field, the parameter Λ is equivalent to a renormalized coupling efficiency for $\phi = 0$. In particular, even if η is small, one can tune Ω_{pump} to obtain $\Lambda = 1/2$, achieving the previous perfect attenuation $T = 0$. Note that $T = 0$ does not imply that the total field of Eq. (2) generally has zero intensity in the forward direction. Rather, the zero transmission into the detection (probe) mode only implies that the total field is orthogonal to the Gaussian detection mode, while the total field may continue to transport energy in the forward direction, e.g., in higher-order Laguerre-Gauss modes. This is allowed because the atomic radiation pattern is only partially matched to the Gaussian mode. We emphasize that the calculations throughout this work have been performed in the weak driving regime, and thus this attenuation is a purely linear optical phenomenon. Physically, since the pump and probe have the same frequency, they are indistinguishable from the standpoint of the atom, which only sees their combined amplitude. The total driving field then induces an oscillating atomic dipole moment $d_{ge}\langle\hat{\sigma}^{ge}\rangle$, whose radiated field into the detection mode perfectly and destructively interferes with the input probe beam (Fig. 1). Of course, the addition of a sufficiently strong pump can also increase the total number of photons in the collection direction to exceed the number of input probe photons, causing $T > 1$.

The ability to tune the effectively enhanced coupling Λ is illustrated in Fig. 2, where we plot the spectrum for

the transmission coefficient T, first for no pump ($\Omega_{\text{pump}} = 0$) and a coupling efficiency $\eta = 0.05$ similar to the one measured in the single-atom experiment of Ref. [12] [Fig. 2(a)]. We have generalized the above calculations to allow for a nonzero detuning $\Delta = \omega_{\text{p}} - \omega_{ge}$ between the incoming probe and atomic resonance frequency ω_{ge} [Eq. (8) is obtained for $\Delta = 0$]. A minimum transmittance on resonance of $T \approx 80\%$ is predicted, as seen in experiments. In Fig. 2(b), we then increase Λ to $\{0.25, 0.5, 1.1\}$ by increasing the pump amplitude. One can observe the complete attenuation of transmission for $\Lambda = 1/2$, and also the bump in transmission $T > 1$ for values of $\Lambda > 1$.

B. Photon number correlations

Having discussed the effects of the pump beam on the transmission spectra, we continue with the second-order correlation function $g^{(2)}(\tau)$, which characterizes the relative likelihood of detecting two photons separated by a time delay τ and is defined as

$$g^{(2)}(\tau) = \frac{\langle \hat{E}^{\dagger}_{\text{det}}(0)\hat{E}^{\dagger}_{\text{det}}(\tau)\hat{E}_{\text{det}}(\tau)\hat{E}_{\text{det}}(0)\rangle}{|\langle \hat{E}^{\dagger}_{\text{det}}(0)\hat{E}_{\text{det}}(0)\rangle|^2}, \tag{9}$$

where the denominator can be obtained from Eq. (8) using $\langle \hat{E}^{\dagger}_{\text{det}}(0)\hat{E}_{\text{det}}(0)\rangle = T\Phi_{\text{p}}$. The numerator of Eq. (9) is calculated by moving to the Schrödinger picture, where it physically describes a process in which, starting from the steady-state density matrix $\hat{\rho}_{\text{ss}}$, a photon is detected at time $\tau = 0$, which projects the atom into a new conditional state $\hat{\rho}'(0) = \hat{E}_{\text{det}}\hat{\rho}_{\text{ss}}\hat{E}^{\dagger}_{\text{det}}/\text{Tr}(\hat{E}_{\text{det}}\hat{\rho}_{\text{ss}}\hat{E}^{\dagger}_{\text{det}})$. Note that the annihilation operator $\hat{E}_{\text{det}}$ is the coherent sum of the probe and the scattered field as represented by the atomic lowering operator. The resulting interference and detection of a photon gives rise to a nontrivial state, which in particular is not just $\hat{\rho}'(0) = |g\rangle\langle g|$, as would be the case if a purely scattered photon was detected. The numerator of Eq. (9) then corresponds to the intensity emitted by the system, $\text{Tr}[\hat{E}^{\dagger}_{\text{det}}\hat{E}_{\text{det}}\hat{\rho}'(\tau)]$, as this transient density matrix evolves in time τ under Eq. (1), eventually returning back to the steady state. It is straightforward to show that

$$g^{(2)}(\tau) = e^{-\Gamma_0\tau}\left[\left|\frac{2\Lambda}{1-2\Lambda}\right|^2 - e^{\Gamma_0\tau/2}\right]^2, \tag{10}$$

within the weak driving approximation. The form of Eq. (10) has been previously derived for the case of no pump field ($\Lambda = \eta$) [2,12,28], and remains unchanged in the presence of a pump, with the coupling efficiency replaced by $\Lambda = \eta\Omega/|\Omega_{\text{probe}}|$. That is, from the standpoint of transmission [Eq. (8)] and also second-order correlation function [Eq. (10)], the addition of a pump beam plays *exactly the same role* as achieving a higher coupling efficiency, within the weak driving regime and assuming mutually orthogonal pump-probe spatial modes. This constitutes the central result of this work.

Next, we study the $g^{(2)}(\tau)$ within different regimes of interest using Eq. (10). For no pump beam ($\Lambda = \eta$) and low coupling efficiency of $\eta = 0.05$, the statistics of the total detected field are naturally dominated by the one from the coherent input probe, such that $g^{(2)}(\tau) \approx 1$ [Fig. 3(a)]. On the other hand, by tuning the pump such that $\Lambda = 1/2$, one can achieve extreme bunching at zero time delay,

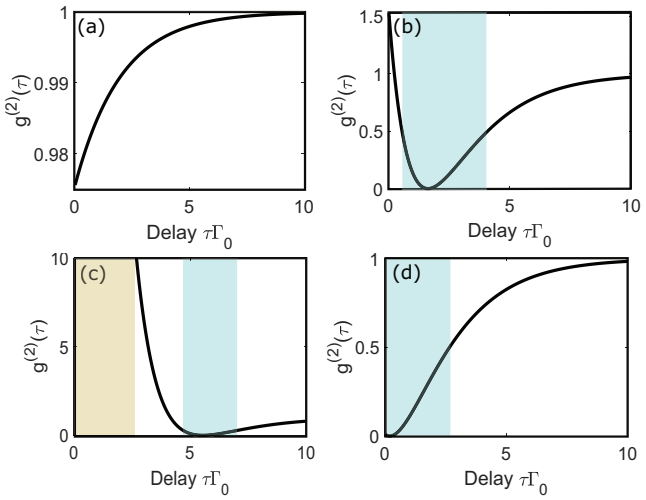

FIG. 3. Second-order correlation function $g^{(2)}(\tau)$ of the transmitted field for a weak, coherent probe beam, as a function of time delay τ scaled by the free-space decay rate Γ_0. In (a) the pump amplitude is set to zero and we take an experimentally realistic atom-light coupling efficiency of $\eta = 0.05$. Due to the low coupling efficiency, the transmitted field mostly consists of the incident coherent field, and thus $g^{(2)}(\tau) \approx 1$ at all times τ. In (b) and (c), a nonzero pump yields an effectively enhanced coupling efficiency of $\Lambda = 0.3$ and $\Lambda = 0.4$ (respectively), giving rise to nontrivial photon correlations. In (d) we consider the case of $\Lambda = 10$, where a pump beam much stronger than the probe causes the total field correlations to be dominated by the atomic scattered field, which is trivially antibunched. Light blue regions correspond to notably antibunched correlations ($g^{(2)} < 0.5$), while light yellow is used to indicate large photon bunching ($g^{(2)} > 10$).

$g^{(2)}(0) \to \infty$. More precisely, an exact calculation shows that $g^{(2)}(0) \propto (\Gamma_0/\Omega)^4$, as the Rabi frequency is reduced. The large bunching coincides with the suppression of the linear transmission $T = 0$ in the denominator of Eq. (9). Physically, with the complete cancellation of the linear response, the remaining photons detected in $g^{(2)}$ are those arising from nonlinear processes, where the atom acts as a frequency mixer and the rescattered photons propagate past the atom in a correlated fashion [29,30]. Furthermore, in cases where strong bunching is observed at $\tau = 0$, a perfect antibunching $g^{(2)}(\tau) = 0$ of the photon correlations can be found at later delay times $\tau_A = (4/\Gamma_0)\ln|2\Lambda/(2\Lambda - 1)|$ [Figs. 3(b) and 3(c)]. The expression for τ_A holds for the parameter regime $1/4 \leqslant \Lambda < 1/2$ and, in particular, for $\Lambda = 1/4$, one finds perfect antibunching at $\tau_A = 0$. As we discuss later, this can be understood from the transient atomic state following the detection of the first photon, which happens to instantaneously emit light with an amplitude and phase that cancels the probe beam, before relaxing back to equilibrium. Finally, for large values of $\Lambda \gg 1$, the scattered field dominates over the probe, giving rise to the characteristic antibunching of the pure atomic emission [Fig. 3(d)]. Note that Λ can be arbitrarily large without saturating the atomic response. In particular, for a given weak pump, one can always find a sufficiently weaker probe such that Λ is large and the weak driving approximation is still valid.

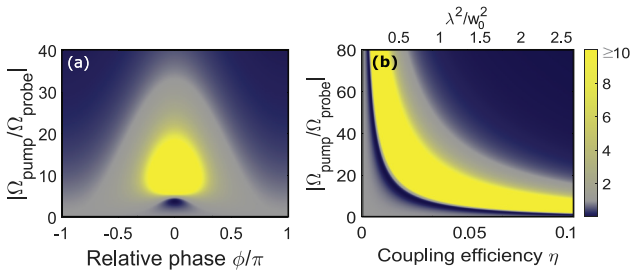

FIG. 4. Second-order correlation function $g^{(2)}(0)$ as a function of the coupling efficiency η, the pump-probe relative phase ϕ, and the amplitude ratio $|\Omega_{\text{pump}}/\Omega_{\text{probe}}|$. In (a) we fix $\eta = 0.05$ and plot $g^{(2)}(0)$ as a function of $|\Omega_{\text{pump}}/\Omega_{\text{probe}}|$ and ϕ. In (b) we show again the values of $g^{(2)}(0)$ but now fixing $\phi = 0$ and exploring different η. Additionally, we show the beam waist w_0 associated to the values of η assuming a spatial Gaussian detection mode within the paraxial approximation. As extreme values of bunching are possible, we represent all the values $g^{(2)}(0) \geqslant 10$ by the same color.

Overall, a proper tuning of the pump field allows one to switch from completely antibunched to extremely bunched photon correlations. While thus far we considered a fixed relative pump-probe phase $\phi = 0$, we can alternatively plot the $g^{(2)}(0)$ for varying amplitude $|\Omega_{\text{pump}}|$ and relative phase, as shown in Fig. 4(a) (for a fixed $\eta = 0.05$). It can be seen that the strong antibunching and bunching features exist within a reasonable tolerance of the relative phases and amplitudes. Likewise, in Fig. 4(b), we consider a fixed relative phase $\phi = 0$ and vary η. For reference, we also provide the beam waist w_0 corresponding to this coupling efficiency, assuming a paraxial, Gaussian detection mode (where $\eta = 3\lambda^2/8\pi^2 w_0^2$).

IV. CONNECTION WITH THE TRANSIENT ATOMIC STATE

In this section, we present an alternative description for the origin of the second-order correlations, now from the atomic state perspective. As shown in the previous section, starting from the steady state, the detection of a photon at $t = 0$ projects the atom into the new conditional state $\hat{\rho}'(0)$ (which in general is different from the ground state). With this, $g^{(2)}(\tau)$ is then related to the average intensity of the conditioned total transmitted field since $g^{(2)}(\tau) = \langle \hat{E}^\dagger_{\text{det}} \hat{E}_{\text{det}} \rangle_{\hat{\rho}'(\tau)}/T$, with $\hat{\rho}'(\tau)$ obeying Eq. (1). It is helpful to explicitly write out the solution to the transient atomic coherence,

$$\hat{\rho}'_{ge}(\tau) = \frac{-2i\Omega}{\Gamma_0}\left(1 + \frac{2\Lambda}{1-2\Lambda} e^{-\Gamma_0 \tau/2}\right), \tag{11}$$

where we again neglect terms of order Ω^2. The population in the excited state can be obtained through $\hat{\rho}'_{ee}(t) = |\hat{\rho}'_{ge}(t)|^2$ within the weak driving approximation. From Eq. (11), the atomic coherence of the new state right after the detection of a photon reads $\hat{\rho}'_{ge}(0) = -2i\Omega/[\Gamma_0(1-2\Lambda)]$. Then, for no pump and small η, one can see that $\hat{\rho}'_{ge}(0) \approx \hat{\rho}^{\text{ss}}_{ge}$ as the first photon measurement barely affects the atom. For $\Lambda = 1/4$ (perfect antibunching), the atom is projected into a conditional state whose scattered field cancels the input probe amplitude at $\tau = 0$, as can be confirmed by substituting the conditional atomic coherence $\hat{\rho}'_{ge}(0)$ into Eq. (5). If $\Lambda > 1/4$, the conditional total field has the opposite sign at $\tau = 0$ compared to its steady-state value. Thus, as it relaxes back to equilibrium, $g^{(2)}(\tau)$ becomes antibunched at $\tau = \tau_A$, when the conditional total field switches sign and passes through zero.

Exactly at $\Lambda = 1/2, T = 0$ for the system in its steady state [see Eq. (8)], as the scattered field completely cancels the input probe at the linear optics level. This implies that individual photons cannot be transmitted through the atom. Instead, the only transmission events for weak driving consist of photon pairs, which are frequency mixed by the atom. The individual photons of this pair have no well-defined phase, but are frequency correlated with each other [29,30]. This lack of phase is reflected in the conditional atomic density matrix. In this case, the linear approximation $\hat{\rho}'_{ge}(0) = -2i\Omega/[\Gamma_0(1-2\Lambda)]$ breaks down, and an exact calculation reveals that the atom is completely mixed, with $\hat{\rho}'_{ee}(0) = \hat{\rho}'_{gg}(0) = 1/2$.

V. EXPERIMENTAL CONSIDERATIONS

Thus far, our analysis has been restricted to idealized conditions, such as a two-level atomic structure and fixed efficiency η (indicating the absence of atomic motion within the beam). Here, we analyze more carefully the roles of uncertainty in atomic position and realistic atomic hyperfine structure. First, we address the effect of randomness in the atomic position, which will necessarily arise from the finite trap extent, nonzero motional temperature, and even quantum zero-point fluctuations. To be specific, we consider that both the probe and pump fields are focused Gaussian beams, with spatial profile described by Eq. (6). In particular, we take the propagation directions of the probe and pump beams to be along y and z, respectively. We will then calculate and plot the transmission T and second-order correlation function $g^{(2)}(0)$ for displacements of the atomic position in the two-dimensional y-z plane, so that, in Eq. (6), (ρ, ζ) is $(-z, y)$ for the probe and (y, z) for the pump [see Fig. 5(c)]. Formally, all previous results remain the same. However, the effective coupling parameter $\Lambda(\mathbf{r}_d)$ and probe coupling efficiency $\eta(\mathbf{r}_d)$ now become position-dependent, according to $\Lambda(\mathbf{r}_d) = \eta(\mathbf{r}_d)\Omega(\mathbf{r}_d)/|\Omega_{\text{probe}}(\mathbf{r}_d)|$ and $\eta(\mathbf{r}_d) = 3|\mathbf{E}_{\text{det}}(\mathbf{r}_d) \cdot \mathbf{d}|^2/2k_0^2 w_0^2 |\mathbf{E}_{\text{det}}(0)|^2$.

Figure 5 shows the spatially dependent transmission $T(\mathbf{r}_d)$ and second-order correlation function $g^{(2)}(t = 0; \mathbf{r}_d)$, i.e., Eqs. (8) and (10), respectively, for different displacements $\mathbf{r}_d = (\Delta y, \Delta z)$ of the atomic position within the y-z plane. For concreteness, we choose the beam waists of the pump and probe beams to be $w_0 \approx 0.9\lambda$ such that the coupling efficiency at the origin $\eta(0) = 0.05$. We further choose the pump beam intensity so that the effective coupling parameter $\Lambda(0) = 1/2$ at the origin. Then, placing the atom at the origin, the linear transmission of the probe is completely suppressed and $g^{(2)}(0; 0)$ is maximal (divergent). In Figs. 5(b) and 5(c), it can be seen that all interesting features in transmission and $g^{(2)}(0; \mathbf{r}_d)$ gradually become washed out for atomic displacements greater than the beam waist $\Delta y, \Delta z \gtrsim w_0$. Additionally, a much finer interference fringe pattern appears. This arises from the spatially varying relative phases between the pump and the probe fields. Near the origin, constant relative phases and maximum relative phase gradients are obtained along the lines $\Delta z = \Delta y$ and $\Delta z = -\Delta y$, respectively. Defining the

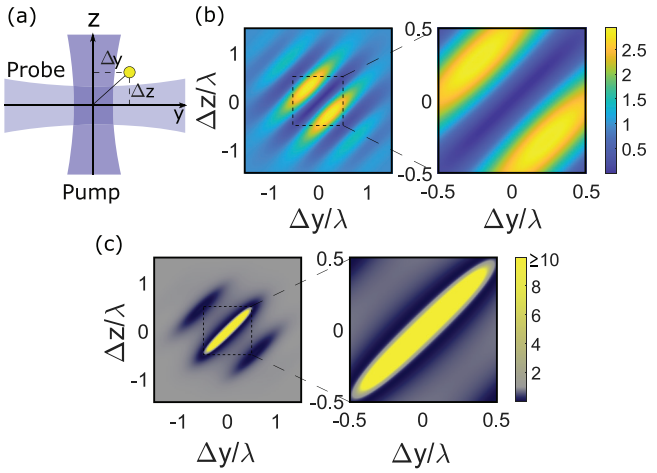

FIG. 5. (a) Schematic representation of an atom displaced by an amount $\mathbf{r}_d = (\Delta y, \Delta z)$ from the origin, which also constitutes the common focal point of the probe and pump beams propagating along y and z, respectively. (b),(c) Transmission $T(\mathbf{r}_d)$ (b) and second-order correlation function $g^{(2)}(0; \mathbf{r}_d)$ (c) for different atomic displacements $\mathbf{r}_d = (\Delta y, \Delta z)$. The amplitude, beam waists, and phase of the pump and probe fields are chosen such that $\eta(0) = 0.05$ and $\Lambda(0) = 1/2$ at the focal point. Central regions of (b) and (c) are also shown magnified.

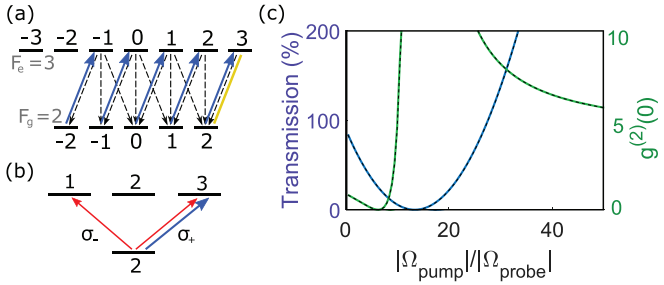

FIG. 6. (a) Energy levels of the maximum angular momentum ground- and excited-state manifolds of ^{87}Rb, with $F_g = 2$ and $F_e = 3$, respectively. Each manifold has $2F_{g(e)} + 1$ hyper-fine levels labeled by $m_{g(e)} \in [-F_{g(e)}, F_{g(e)}]$. The dashed lines indicate the allowed decay paths of the excited states, while the blue lines represent the transitions driven by a strong pump field with σ_+ polarization. For clarity, the transitions of the x-polarized probe field are not indicated here. In the steady state, the strong pump nearly perfectly restricts the population within the cycling transition involving states $|F_e = 3, m_e = 3\rangle$ and $|F_g = 2, m_g = 2\rangle$ (golden line). (b) Illustration of the most relevant states. The strong pump restricts most of the population to the cycling transition $|F_e = 3, m_e = 3\rangle \rightarrow |F_g = 2, m_g = 2\rangle$, as stated earlier. The weak probe (red) has polarization $x = (\sigma_- - \sigma_+)/\sqrt{2}$, while the pump field (blue) is σ_+ polarized. Under the conditions relevant to our scheme, the amount of population driven out of the two-level subspace, to $|F_e = 3, m_e = 1\rangle$, is negligible. (c) Transmission T (blue) and second-order correlation function $g^{(2)}(0)$ (green) for a multilevel atom as a function of the pump-probe amplitude ratio. The solid lines are obtained from Eqs. (8) and (10) after substituting the coupling parameter $\bar{\eta}$ and taking into account the suggested pump and probe polarizations. The dashed lines are obtained with a numerical simulation considering all the hyperfine levels in (a). In the simulations, we take $\bar{\eta} = 0.025$.

rotated coordinate $\zeta_- = (y - z)/\sqrt{2}$ along the direction of the phase gradient, it can be seen [Figs. 5(b) and 5(c)] that a position uncertainty of $\Delta\zeta_- \approx \lambda/10$ allows one to observe strong suppression of the transmission and large bunching in the entire spatial region. In the case of the D_2 line of ^{87}Rb, such localization could be achieved, for instance, with a realistic [17,31] trap frequency of $\omega = 2\pi \times 100$ kHz and a motional temperature of $\mathcal{T} = 20\ \mu$K.

Having discussed the external degrees of freedom, next we refine our model for the atomic internal levels. Instead of a single ground and excited state, most atoms have a richer internal structure involving several hyperfine levels. In particular, we consider the case when the dynamics of a multilevel atom can effectively be restricted to a single ground- and excited-state manifold with total hyperfine angular momenta F_g and $F_e = F_g + 1$, respectively. By choosing F_g to be the maximum allowed value, excitation to F_e necessarily results in emission back to F_g, such that the atomic population always remains in this manifold. We illustrate this in Fig. 6(a) in the case of the D_2 line of ^{87}Rb, where $F_g = 2$ and $F_e = 3$. The label for the atomic states is completed with the projection of their angular momentum along the z axis, such that we use $|F_g, m_g\rangle$ for the ground states and $|F_e, m_e\rangle$ for the excited ones, with $m_{e(g)} \in [-F_{e(g)}, F_{e(g)}]$. The ground and excited states couple following the selection rule $m_e = m_g + q$, where $q = \{0, \pm 1\}$ denotes the angular momentum of the photon involved in the transition [32]. We define $\hat{\epsilon}_q$ as the polarization of said photon expressed in the complex spherical basis

$$\hat{\epsilon}_q = \begin{cases} q = 1, & \sigma_+ = -(\mathbf{x} + i\mathbf{y})/\sqrt{2}, \\ q = 0, & \sigma_0 = \mathbf{z}, \\ q = -1, & \sigma_- = (\mathbf{x} - i\mathbf{y})/\sqrt{2}. \end{cases} \tag{12}$$

To recover the results derived in the ideal two-level picture, we propose the polarization scheme illustrated in Fig. 6(b), where the pump and probe fields have polarizations σ_+ and $\mathbf{x} = (\sigma_- - \sigma_+)/\sqrt{2}$, respectively. In this configuration, the strong pump field (which is needed anyway for our proposed scheme) also serves to optically pump the atomic population into the cycling transition $|F_e, F_e\rangle \leftrightarrow |F_g, F_g\rangle$ [see Figs. 6(a) and 6(b)]. In other words, the atomic Hilbert space is effectively restricted to a two-level subspace, which enables one to directly apply our previous two-level analysis to an excellent approximation. The degree to which the system retains a two-level nature can be estimated by the ratio of populations in the $|F_e, F_e\rangle$ and $|F_e, F_e - 2\rangle$ excited states, with the latter being weakly populated due to the partial σ_- polarization component from the probe beam. This ratio is roughly $\sim |C^{F_g}_{F_e}(\mathbf{E}_T \cdot \sigma_+)|^2 / |C^{F_g}_{F_e-2}(\mathbf{E}_T \cdot \sigma_-)|^2$. Here, $\mathbf{E}_T = \mathbf{E}_{\text{pump}} + \mathbf{E}_{\text{probe}}$ is the total field driving the atom and $C^{m_g}_{m_e}$ are the Clebsch-Gordan coefficients associated to the transitions $|F_g, m_g\rangle \leftrightarrow |F_e, m_e\rangle$. For ^{87}Rb, the squared ratio of the Clebsch-Gordan coefficient is $|C^2_3|^2/|C^2_1|^2 = 15$ [33], and, furthermore, the pump intensity needs to be approximately $\sim 10^2$ larger than the probe to achieve the desired phenomena. The amount of population not residing in the restricted two-level subspace can then realistically be on the level of $\sim 10^{-3}$.

Since the multilevel atom now behaves as an effective two-level system, the transmission T and second-order correlation function $g^{(2)}(0)$ can be approximated by Eqs. (8) and (10), respectively. However, because of the probe polarization, the coupling efficiency $\bar{\eta}$ and probe Rabi frequency Ω_{probe} are reduced by a factor of two and $\sqrt{2}$, respectively, compared to the ideal case of a probe beam polarized along the two-level transition (Sec. III). In Fig. 6(c), we plot T and $g^{(2)}(0)$ from Eqs. (8) and (10) as a function of the ratio $|\Omega_{\text{pump}}|/|\Omega_{\text{probe}}|$, after substituting $\bar{\eta}$. For this calculation, we assume that the atom is fixed at the origin and we take the beam waists such that the coupling efficiency is $\bar{\eta} = 0.025$ (or $\eta = 0.05$ for an ideal probe polarization). To quantitatively verify the validity of this simplified, effective two-level model, we have also performed a density-matrix calculation using the whole $F_g = 2$ and $F_e = 3$ manifolds of the D_2 line in ^{87}Rb. The master equation of the system [Eq. (1)] and the total field input-output equations [Eqs. (2) and (5)] can be readily generalized to the multilevel case following Refs. [32,34], which we do not explicitly write here to avoid a significant increase in notational complexity. It can be seen that the full master equation and the modified effective two-level description produce excellent agreement, thus justifying the latter model.

VI. CONCLUSIONS

We have described a scheme in which a single, laser-illuminated atom can produce strongly nonclassical photon correlations in the total field. Considering two laser beams that meet at the atom, we find scenarios in which the detected atomic contribution can easily be made comparable in strength to the detected laser contribution. We show that the effect of the second beam, which acts as a pump, is in some scenarios formally equivalent to an increased atom-light coupling efficiency. This allows one to achieve correlations associated with coupling efficiencies beyond what is practically possible, and even beyond what is physically possible, i.e., above 100%. We expect that our method can be immediately applied to observe interesting quantum behavior in existing experiments where single atoms are coupled to tightly focused beams. It would also be interesting in the future to explore more broadly whether other single-atom, quantum scattering phenomena can be effectively "amplified" by similar techniques.

ACKNOWLEDGMENTS

We thank S. Grava and H. J. Kimble for valuable discussions. The authors acknowledge funding from the following: Spanish MINECO projects OCARINA (Grant Ref. No. PGC2018-097056-B-I00), Q-CLOCKS (No. PCI2018-092973), ALIQS (No. PGC2018-096844-B-I00), and MINECO Severo Ochoa Grant No. CEX2019-000910-S; Fundación Ramón Areces Project CODEC; Fundacio Mir-Puig; Fundacio Privada Cellex; Agència de Gestió d'Ajuts Universitaris i de Recerca (AGAUR) Projects (No. 2017-SGR-1334 and No. 2017-SGR-1354); Generalitat de Catalunya (CERCA Programme, RIS3CAT project QuantumCAT); the Secretaria d'Universitats i Recerca de la Generalitat de Catalunya and the European Social Fund (2020 FI B 00196); the European Research Council under the European Union's Horizon 2020 research and innovation programme (Grant Agreement No. 101002107 (NEWSPIN)); and Quantum Technology Flagship projects MACQSIMAL (820393) and QRANGE (820405). This project 17FUN03 USOQS has received funding from the EMPIR programme co-financed by the Participating States and from the European Union's Horizon 2020 research and innovation programme.

APPENDIX: DERIVATION OF THE MODE-PROJECTED OPERATORS

Here we derive the projection of $\hat{\mathbf{E}}_{\text{out}}(\mathbf{r})$, Eq. (5) in the main text, starting from Eq. (2), following closely the arguments in Ref. [22]. The quantized electromagnetic field can be expressed as a combination of plane-wave operators of the form $\hat{\mathbf{E}}_{\mathbf{k},\hat{\epsilon}_{\mathbf{k},j}}(\mathbf{r}) = E_0(k)\mathbf{u}_{\mathbf{k},\hat{\epsilon}_{\mathbf{k},j}}(\mathbf{r})\hat{a}_{\mathbf{k},\hat{\epsilon}_{\mathbf{k},j}}$, labeled by the wave-vector $\mathbf{k}$ and the orthonormal polarizations $\hat{\epsilon}_{\mathbf{k},j}$ with $j = \{1, 2\}$ and $\mathbf{k} \cdot \hat{\epsilon}_{\mathbf{k},j} = 0$. Here, we define $\mathbf{u}_{\mathbf{k},\hat{\epsilon}_{\mathbf{k},j}}(\mathbf{r}) = e^{-i\mathbf{k}\cdot\mathbf{r}}\hat{\epsilon}_{\mathbf{k},j}$ as the plane-wave spatial mode, $\hat{a}_{\mathbf{k},\hat{\epsilon}_{\mathbf{k},j}}$ is the associated photon annihilation operator, and $E_0(k)$ is a normalization factor, whose specific form is not relevant here. For a fixed $|\mathbf{k}| = k_0$, one can alternatively construct a field operator $\hat{\mathbf{E}}_\alpha(\mathbf{r})$ based on any superposition of plane waves of the same $|\mathbf{k}|$,

$$\hat{\mathbf{E}}_\alpha(\mathbf{r}) = E_0(k_0)\hat{a}_\alpha\mathbf{E}_\alpha(\mathbf{r}), \tag{A1}$$

where the associated spatial mode reads

$$\mathbf{E}_\alpha(\mathbf{r}) = \frac{k_0^2}{(2\pi)^2}\sum_{j=1,2}\int_0^{2\pi} d\phi \int_0^{\pi} \sin\theta\, d\theta\, c_{\alpha,\theta,\phi,j} \times e^{-ik_0(x\,\sin\theta\,\cos\phi + y\,\sin\theta\,\sin\phi + z\,\cos\theta)}\hat{\epsilon}_{k_0,j}. \tag{A2}$$

Here, we have utilized the spherical coordinates $k_x = k_0 \sin\theta\, \cos\phi$, $k_y = k_0 \sin\theta\, \sin\phi$, $k_z = k_0 \cos\theta$, and $dV_k = k_0^2 \sin\theta\, d\theta\, d\phi$ to express the linear combination as an integral over solid angle. The scalar product (mode overlap) between two arbitrary spatial modes $\mathbf{E}_\alpha(\mathbf{r})$ and $\mathbf{E}_\beta(\mathbf{r})$ is defined as the two-dimensional integral over any fixed plane $z = \text{const}$,

$$\langle\mathbf{E}_\alpha|\mathbf{E}_\beta\rangle \equiv \iint_{z=\text{const}} d^2\mathbf{r}\, \mathbf{E}_\alpha^*(\mathbf{r}) \cdot \mathbf{E}_\beta(\mathbf{r}), \tag{A3}$$

where the plane-wave modes fulfill the orthonormality relation

$$\langle\mathbf{u}_{k_0,\phi',\theta',j'}|\mathbf{u}_{k_0,\phi,\theta,j}\rangle = \frac{(2\pi)^2\delta^{jj'}}{k_0^2\sin\theta}\delta(\theta - \theta')\delta(\phi - \phi'). \tag{A4}$$

The spatial mode overlap from Eq. (A3) can be related to the electromagnetic field power P defined as the integral of the z component of the Poynting vector in the plane $z = 0$. Explicitly,

$$P_\alpha = 2\epsilon_0 c \int_{z=0} d^2\mathbf{r}\, \mathbf{E}_\alpha^*(\mathbf{r}) \cdot \mathbf{E}_\alpha(\mathbf{r}) = 2\epsilon_0 c\, \langle\mathbf{E}_\alpha|\mathbf{E}_\alpha\rangle. \tag{A5}$$

From here, the field operators can be conveniently renormalized such that expectation values of the form $\langle\hat{E}_\alpha^\dagger\hat{E}_\alpha\rangle$ are in units of photons per unit time. To do so, we start by considering a field $\hat{E}_{\text{det}}(\mathbf{r})$ in the spatial detection mode $\mathbf{E}_{\text{det}}(\mathbf{r})$. Multiplying the fields by the normalization constant N, we impose that $\langle N\hat{E}_{det}^\dagger N\hat{E}_{det}\rangle \equiv P_{\text{det}}/\hbar\omega_{ge}$ yielding

$N = \sqrt{2\epsilon_0/\hbar k_0 F_{\rm det}}$, where $F_{\rm det} = |\langle \mathbf{E}_{\rm det}|\mathbf{E}_{\rm det}\rangle|$. This normalization will be implicit for the rest of this section.

Next, we apply the previous ideas to evaluate the projection of the atomic scattered field operator $\hat{\mathbf{E}}_{\rm sc}(\mathbf{r})$ [second term in Eq. (2)] into any desired detection mode $\mathbf{E}_{\rm det}(\mathbf{r})$, using Eq. (A2) and Eq. (A3), by writing both the Green's function and detection mode in a plane-wave expansion [22]. This gives, within the previous normalization,

$$\langle \mathbf{E}_{\rm det}|\hat{\mathbf{E}}_{\rm sc}\rangle = i d_{ge}\sqrt{\frac{k_0}{2\hbar\epsilon_0 F_{\rm det}}}\mathbf{E}^*_{\rm det}(\mathbf{r}_{\rm a})\cdot\mathbf{d}\,\hat{\sigma}^{ge}, \tag{A6}$$

where $\mathbf{E}^*_{\rm det}(\mathbf{r}_{\rm a})$ is the conjugate of the amplitude of the spatial detection mode evaluated at the atomic position $\mathbf{r}_a$. We note that, although the mode function $\mathbf{E}_{\rm det}(\mathbf{r})$ can be arbitrarily rescaled by a global coefficient, this freedom is eliminated in Eq. (A6) through the normalization constant $F_{\rm det}$, thus making the result of the overlap clearly defined. In the case that $E_{\rm det}(\mathbf{r}_a) \propto e^{i\theta(\mathbf{r}_a)}$ contains a complex phase at the atomic location, we will remove this phase by applying a unitary transformation $\hat{U} = e^{i\theta(\mathbf{r}_a)/2}\hat{\sigma}^{gg} + e^{-i\theta(\mathbf{r}_a)/2}\hat{\sigma}^{ee}$ to all atomic operators. At the level of the transformed Hamiltonian $\hat{H} \to \hat{U}\hat{H}\hat{U}^\dagger$, this has the effect of making the Rabi frequency associated with the detection mode real and positive.

Now, we will show that Eq. (A6) can be written in an even simpler way, involving only the collection efficiency η defined as the probability that a photon emitted by the atom is measured in the detection mode. For convenience, we consider the scenario where the atom starts in the excited state and it is not driven by any field, such that $\hat{\rho}^{ee}(t) = e^{-\Gamma_0 t}$ and a single photon is emitted as $t \to \infty$. The explicit value of η is then given by the time integral of the overlap from Eq. (A6),

$$\eta = \int_0^\infty dt\,|\langle \mathbf{E}_{\rm det}|\hat{\mathbf{E}}_{\rm sc}(t)\rangle|^2 = \frac{3\pi}{2k_0^2}\frac{|\mathbf{E}_{\rm det}(\mathbf{r}_{\rm a})\cdot\mathbf{d}|^2}{F_{\rm det}}. \tag{A7}$$

For a detection mode that matches exactly the radiation pattern of a point dipole over 4π (all solid angle), one obtains a maximum of $\eta = 1$. We notice that Eq. (A7) allows us to establish the relation $\sqrt{\Phi_{\rm p}} = |\Omega_{\rm probe}|/\sqrt{\eta\Gamma_0}$ from the main text, as $\Phi_{\rm p} = 2\epsilon_0 c|\langle \mathbf{E}_{\rm p}|\mathbf{E}_{\rm p}\rangle|/\hbar\omega_{ge}$ for the probe beam in the detection mode. Substituting the collection efficiency η from Eq. (A7) into Eq. (A6), we arrive at Eq. (5) in the main text.

[1] M. Dagenais and L. Mandel, Phys. Rev. A **18**, 2217 (1978).
[2] D. E. Chang, A. S. Sørensen, E. A. Demler, and M. D. Lukin, Nat. Phys. **3**, 807 (2007).
[3] S. J. van Enk and H. J. Kimble, Phys. Rev. A **61**, 051802(R) (2000).
[4] E. Rephaeli and S. Fan, Phys. Rev. Lett. **108**, 143602 (2012).
[5] V. Rupasov and V. Yudson, Sov. Phys. JETP **59**, 478 (1984).
[6] J.-T. Shen and S. Fan, Phys. Rev. Lett. **98**, 153003 (2007).
[7] S. Mahmoodian, G. Calajó, D. E. Chang, K. Hammerer, and A. S. Sørensen, Phys. Rev. X **10**, 031011 (2020).
[8] M. K. Tey, G. Maslennikov, T. C. H. Liew, S. A. Aljunid, F. Huber, B. Chng, Z. Chen, V. Scarani, and C. Kurtsiefer, New J. Phys. **11**, 043011 (2009).
[9] S. J. van Enk and H. J. Kimble, Phys. Rev. A **63**, 023809 (2001).
[10] M. K. Tey, Z. Chen, S. A. Aljunid, B. Chng, F. Huber, G. Maslennikov, and C. Kurtsiefer, Nat. Phys. **4**, 924 (2008).
[11] B. Darquié, M. P. A. Jones, J. Dingjan, J. Beugnon, S. Bergamini, Y. Sortais, G. Messin, A. Browaeys, and P. Grangier, Science **309**, 454 (2005).
[12] Y. Chin, M. Steiner, and C. Kurtsiefer, Nat. Commun. **8**, 1200 (2017).
[13] H. J. Kimble, Phys. Scr. **T76**, 127 (1998).
[14] A. Reiserer and G. Rempe, Rev. Mod. Phys. **87**, 1379 (2015).
[15] A. Goban, C.-L. Hung, S.-P. Yu, J. D. Hood, J. A. Muniz, J. H. Lee, M. J. Martin, A. C. McClung, K. S. Choi, D. E. Chang, O. Painter, and H. J. Kimble, Nat. Commun. **5**, 3808 (2014).
[16] M. Arcari, I. Söllner, A. Javadi, S. Lindskov Hansen, S. Mahmoodian, J. Liu, H. Thyrrestrup, E. H. Lee, J. D. Song, S. Stobbe, and P. Lodahl, Phys. Rev. Lett. **113**, 093603 (2014).
[17] N. Bruno, L. C. Bianchet, V. Prakash, N. Li, N. Alves, and M. W. Mitchell, Opt. Express **27**, 31042 (2019).
[18] H. T. Dung, L. Knöll, and D.-G. Welsch, Phys. Rev. A **66**, 063810 (2002).
[19] A. Asenjo-Garcia, J. D. Hood, D. E. Chang, and H. J. Kimble, Phys. Rev. A **95**, 033818 (2017).
[20] P. Meystre and M. Sargent, *Elements of Quantum Optics* (Springer, Berlin, 1998).
[21] J. D. Jackson, *Classical Electrodynamics*, 3rd ed. (Wiley, New York, 1999).
[22] M. T. Manzoni, M. Moreno-Cardoner, A. Asenjo-Garcia, J. V. Porto, A. V. Gorshkov, and D. E. Chang, New J. Phys. **20**, 083048 (2018).
[23] S. A. Moiseev and S. Kröll, Phys. Rev. Lett. **87**, 173601 (2001).
[24] A. V. Gorshkov, A. André, M. Fleischhauer, A. S. Sørensen, and M. D. Lukin, Phys. Rev. Lett. **98**, 123601 (2007).
[25] C. G. Chen, P. T. Konkola, J. Ferrera, R. K. Heilmann, and M. L. Schattenburg, J. Opt. Soc. Am. A **19**, 404 (2002).
[26] B. R. Mollow, Phys. Rev. A **12**, 1919 (1975).
[27] L. Slodicka, G. Hetet, S. Gerber, M. Hennrich, and R. Blatt, Phys. Rev. Lett. **105**, 153604 (2010).
[28] P. Kochan and H. J. Carmichael, Phys. Rev. A **50**, 1700 (1994).
[29] J.-T. Shen and S. Fan, Phys. Rev. A **76**, 062709 (2007).
[30] T. Caneva, M. T. Manzoni, T. Shi, J. S. Douglas, J. I. Cirac, and D. E. Chang, New J. Phys. **17**, 113001 (2015).
[31] A. Fuhrmanek, A. M. Lance, C. Tuchendler, P. Grangier, Y. R. P. Sortais, and A. Browaeys, New J. Phys. **12**, 053028 (2010).
[32] D. A. Steck, Quantum and Atom Optics, available online at http://steck.us/teaching (revision 0.13.4, 24 September 2020).
[33] D. A. Steck, Rubidium 87 D Line Data, available online at http://steck.us/alkalidata (revision 2.2.2, 9 July 2021).
[34] A. Asenjo-Garcia, H. J. Kimble, and D. E. Chang, Proc. Natl. Acad. Sci. U.S.A. **116**, 25503 (2019).